Available online at www.sciencedirect.com
ScienceDirect
Journal of Sound and Vibration 321 (2009) 510–524
JOURNAL OF SOUND AND VIBRATION
www.elsevier.com/locate/jsvi

Dynamic modelling and active vibration controller design for a cylindrical shell equipped with piezoelectric sensors and actuators

Moon K. Kwak*, Seok Heo, Moonsan Jeong

Department of Mechanical Engineering, Dongguk University, 26 Pil-Dong 3-Ga, Joong-Gu, Seoul 100-715, Korea

Received 27 March 2008; received in revised form 25 June 2008; accepted 30 September 2008
Handling Editor: J. Lam
Available online 18 November 2008

Abstract

This paper is concerned with the dynamic modelling, active vibration controller design and experiments for a cylindrical shell equipped with piezoelectric sensors and actuators. The dynamic model was derived by using Rayleigh–Ritz method based on the Donnel–Mushtari shell theory. The actuator equations which relate the applied voltages to the generalized force and sensor equations which relate the generalized displacements to the sensor output voltages for the piezoelectric wafer were derived based on the pin-force model. The equations of motion along with the piezoelectric sensor equations were then reduced to modal forms considering the modes of interest. An aluminium shell was fabricated to demonstrate the effectiveness of the modelling and control techniques. The boundary conditions at both ends of the shell were assumed to be a shear diaphragm in the numerical analysis. Theoretical natural frequencies of the aluminium shell were then calculated and compared to experimental result. They were in good agreement with experimental result for the first two free-vibration modes. The multi-input and multi-output positive position feedback controller, which can cope with the first two vibration modes, was designed based on the block-inverse theory and was implemented digitally using the DSP board. The experimental results showed that vibrations of the cylindrical shell can be successfully suppressed by the piezoelectric actuator and the proposed controller.

1. Introduction

A smart structure is defined as one that contains distributed sensors and actuators and implements a control scheme to achieve vibration suppression in close cooperation with sensors and actuators. Conceptually, a smart structure should be able to respond to external disturbances and internal changes. Many materials have been tested as actuators and sensor: piezoelectric materials, shape memory alloys, electrostrictive materials, magnetostrictive materials, electro-rheological fluids, and fiber optics. These materials can be inserted into or bonded with structures, thus acting as either a sensor or an actuator. Among them, piezoelectric materials have become popular because of high strength, temperature insensitivity, and ease of implementation.

*Corresponding author. Tel.: +82 2 2260 3705; fax: +82 2 2263 9379.
E-mail address: kwakm@dongguk.edu (M.K. Kwak).

0022-460X/$ - see front matter © 2008 Elsevier Ltd. All rights reserved.
doi:10.1016/j.jsv.2008.09.051

They undergo deformation when applied with a voltage, and produce a charge when deformed. Hence, they can be used as both a sensor and an actuator. In this study, we applied the smart structure technology to the active vibration control of a thin cylindrical shell equipped with piezoelectric sensors and actuators.

A thin cylindrical shell structure has been used as a pressure vessel for storing liquid or gas and as the base structure for submarines. The equations of motion for the cylindrical shell were derived in the work by Arnold and Waburton [1]. Since then, many theories based on different assumptions have been developed for the cylindrical shell [2–4]. Among them, the simplest theory about the behavior of the thin cylindrical shell is the Donnel and Mushtari [2] theory. Active control of sound and vibration of the cylindrical shell using piezoelectric actuators were investigated by Tzou et al. [5], Lester and Lefebvre [6], Sonti and Jones [7], Clark and Fuller [8]. Tzou et al. [5] studied the application of modal piezoelectric actuator for active vibration control of a shell structure. Lester and Lefebvre [6] investigated the coupling between the cylindrical mode and internal acoustic cavity modes using modal spectra and proved theoretically that the piezoelectric actuator can be used for internal cavity noise control. Sonti and Jones [7] developed a simple model for a cylindrical shell with piezoelectric actuators and concluded that a large piezoelectric actuator is more effective than a small one by numerical analysis. Clark and Fuller [8] carried out acoustic control experiments using a piezoceramic actuator, microphone, PVDF sensor mounted on an aluminum shell and the Filtered-x LMS control technique. Their experimental results showed that it is easy to control the accordion type vibration mode but not easy to control the cylindrical vibration mode because the natural frequency of the aluminum shell structure is very high. However, these works did not provide the equations of motion for the cylindrical shell structure suitable for control design.

The most critical problem in applying a piezoceramic actuator to a shell structure is the curvature of the shell. A plate-type piezoceramic wafer cannot be applied to a shell structure because of its brittleness. Recently, a new type of piezoelectric actuator, so called the MFC (Macro Fiber Composite) actuator [9], was developed to enhance actuating performance by utilizing the piezoelectric constant d_{33} instead of d_{31}. An MFC actuator consists of rectangular piezoceramic rods sandwiched between layers of adhesive and electroded polyimide film; therefore, it can be applied to a curved surface. Sohn et al. [10] analyzed the natural vibration characteristics of the cylindrical shell equipped with an MFC actuator using the finite element code and proved theoretically that the LQG controller could be used as an active vibration controller.

In order to design an active vibration controller theoretically for the cylindrical shell, the equations of motion for the shell suitable for control design should be derived a priori. Hence, we first derived a dynamic model for a cylindrical shell equipped with piezoelectric actuators using the assumed-mode method based on the Donnel–Mushtari shell theory. The piezoelectric actuator equations which relate the applied voltage to the generalized forces and the piezoelectric sensor equations which relate the generalized displacements to the sensor output voltage were also derived by assuming the piezoelectric actuator as a pin-force model [11]. An aluminum shell equipped with two MFC actuators was built and its natural frequencies were obtained by the impact hammer test. The active vibration controller based on the multi-input–multi-output positive position feedback (MIMO PPF) control technique [12] was designed using the theoretical model derived in this study and tuned to the natural frequencies found experimentally. The proposed MIMO PPF controller was applied to the test article using the digital controller. The experimental results showed that the vibrations of the shell were suppressed successfully by the MFC actuator and the proposed controller.

2. Kinetic and potential energies for cylindrical shell

Let us derive the dynamic model for the cylindrical shell, as shown in Fig. 1, in which R is the radius of the cylindrical shell, h is the thickness, L is the length, θ is the angle with respect to the vertical axis, x is the axis along its length, u, v, w are displacements in the x, θ and z directions, respectively. The kinetic energy for the cylindrical shell is expressed as [2].

$$T = \frac{1}{2}\rho \int_0^L \int_0^{2\pi} \int_{-h/2}^{h/2} \left(\dot{u}^2 + \dot{v}^2 + \dot{w}^2\right) R \, \mathrm{d}z \, \mathrm{d}\theta \, \mathrm{d}x \tag{1}$$

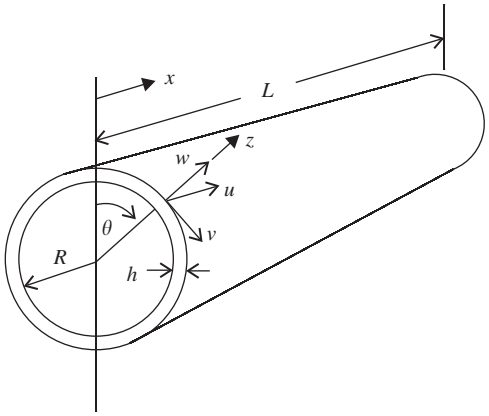

Fig. 1. Coordinate of cylindrical shell.

where ρ is the mass density. Equations for strain and stress are necessary to obtain the potential energy, which are expressed as [2].

$$\varepsilon_x = \frac{\partial u}{\partial x} - z\frac{\partial^2 w}{\partial x^2}, \quad \varepsilon_\theta = \frac{1}{R}\frac{\partial v}{\partial \theta} + \frac{w}{R} - \frac{z}{R^2}\frac{\partial^2 w}{\partial \theta^2}, \quad \varepsilon_{x\theta} = \frac{\partial v}{\partial x} + \frac{1}{R}\frac{\partial u}{\partial \theta} - \frac{2z}{R}\frac{\partial^2 w}{\partial x \partial \theta} \tag{2a–c}$$

$$\varepsilon_{xz} = \varepsilon_{\theta z} = \varepsilon_{zz} = 0 \tag{2d}$$

$$\sigma_x = \frac{E}{1-\nu^2}(\varepsilon_x + \nu\varepsilon_\theta), \quad \sigma_\theta = \frac{E}{1-\nu^2}(\varepsilon_\theta + \nu\varepsilon_x), \quad \sigma_{x\theta} = \sigma_{\theta x} = \frac{E}{2(1+\nu)}\varepsilon_{x\theta} \tag{3a–c}$$

$$\sigma_{xz} = \sigma_{\theta z} = \sigma_{zz} = 0 \tag{3d}$$

where E is the Young's modulus and ν is the Poisson's ratio, respectively. The potential energy is then expressed as [2].

$$V = \frac{1}{2}\int_0^L \int_0^{2\pi} \int_{-h/2}^{h/2} (\sigma_x \varepsilon_x + \sigma_\theta \varepsilon_\theta + \sigma_{x\theta}\varepsilon_{x\theta}) R \, \mathrm{d}x \, \mathrm{d}\theta \, \mathrm{d}z \tag{4}$$

Inserting Eqs. (2) and (3) into Eq. (4) results in the following equation for the potential energy [2].

$$\begin{aligned} V = \frac{ERh}{2(1-\nu^2)}\int_0^L \int_0^{2\pi} \Bigg[& \left(\frac{\partial u}{\partial x}\right)^2 + \frac{h^2}{12}\left(\frac{\partial^2 w}{\partial x^2}\right)^2 + \frac{1}{R^2}\left(\frac{\partial v}{\partial \theta}\right)^2 + \frac{w^2}{R^2} + \frac{h^2}{12R^4}\left(\frac{\partial^2 w}{\partial \theta^2}\right)^2 \\ & + \frac{2}{R^2}\left(\frac{\partial v}{\partial \theta}\right)w + \frac{2\nu}{R}\left(\frac{\partial u}{\partial x}\right)\left(\frac{\partial v}{\partial \theta}\right) + \frac{2\nu}{R}\left(\frac{\partial u}{\partial x}\right)w + \frac{\nu h^2}{6R^2}\left(\frac{\partial^2 w}{\partial x^2}\right)\left(\frac{\partial^2 w}{\partial \theta^2}\right) \\ & + \frac{(1-\nu)}{2}\left(\frac{\partial v}{\partial x}\right)^2 + \frac{(1-\nu)}{2R^2}\left(\frac{\partial u}{\partial \theta}\right)^2 + \frac{(1-\nu)h^2}{6R^2}\left(\frac{\partial^2 w}{\partial x \partial \theta}\right)^2 + \frac{(1-\nu)}{R}\left(\frac{\partial v}{\partial x}\right)\left(\frac{\partial u}{\partial \theta}\right)\Bigg] \mathrm{d}x \, \mathrm{d}\theta \end{aligned} \tag{5}$$

Let us express displacements in each direction as the series of functions which have n circumferential nodes.

$$u(x,\theta,t) = \sum_{n=0}^{\infty} u_n(x,\theta,t), \quad v(x,\theta,t) = \sum_{n=0}^{\infty} v_n(x,\theta,t), \quad w(x,\theta,t) = \sum_{n=0}^{\infty} w_n(x,\theta,t) \tag{6a–c}$$

When $n = 0$, the cylindrical shell vibrates without nodal points and its natural frequencies are high compared to those of the cylindrical shell with circumferential nodal points. Hence, we consider the case when $n \geqslant 1$ in the numerical calculation and control design. Each function in Eq. (6) can be expressed as

$$u_n(x,\theta,t) = \Phi_u(x)[\cos n\theta \, q_{nuc}(t) + \sin n\theta \, q_{nus}(t)] \tag{7a}$$

$$v_n(x,\theta,t) = \Phi_v(x)[\sin n\theta\, q_{nvs}(t) + \cos n\theta\, q_{nvc}(t)] \tag{7b}$$

$$w_n(x,\theta,t) = \Phi_w(x)[\cos n\theta\, q_{nwc}(t) + \sin n\theta\, q_{nws}(t)] \tag{7c}$$

where

$$\Phi_u(x) = [\Phi_{u1}(x) \quad \Phi_{u2}(x)\cdots\Phi_{um}(x)] \tag{7d}$$

$$\Phi_v(x) = [\Phi_{v1}(x) \quad \Phi_{v2}(x)\cdots\Phi_{vm}(x)] \tag{7e}$$

$$\Phi_w(x) = [\Phi_{w1}(x) \quad \Phi_{w2}(x)\cdots\Phi_{wm}(x)] \tag{7f}$$

$$q_{nuc}(t) = [q_{nuc1}(t) \quad q_{nuc1}(t)\cdots q_{nucm}(t)]^{\mathrm{T}} \tag{7g}$$

$$q_{nus}(t) = [q_{nus1}(t) \quad q_{nus1}(t)\cdots q_{nusm}(t)]^{\mathrm{T}} \tag{7h}$$

$$q_{nvc}(t) = [q_{nvc1}(t) \quad q_{nvc1}(t)\cdots q_{nvcm}(t)]^{\mathrm{T}} \tag{7i}$$

$$q_{nvs}(t) = [q_{nvs1}(t) \quad q_{nvs1}(t)\cdots q_{nvsm}(t)]^{\mathrm{T}} \tag{7j}$$

$$q_{nwc}(t) = [q_{nwc1}(t) \quad q_{nwc1}(t)\cdots q_{nwcm}(t)]^{\mathrm{T}} \tag{7k}$$

$$q_{nws}(t) = [q_{nws1}(t) \quad q_{nws1}(t)\cdots q_{nwsm}(t)]^{\mathrm{T}} \tag{7l}$$

in which, $\Phi_u(x)$, $\Phi_v(x)$, $\Phi_w(x)$ represent a matrix consisting of admissible functions in each direction, $q_{nuc}(t)$, $q_{nus}(t)$, $q_{nvs}(t)$, $q_{nvc}(t)$, $q_{nwc}(t)$, $q_{nws}(t)$, are generalized coordinate vectors corresponding to the cosine and sine modes, and m is the number of admissible functions used for the longitudinal expansion. Normally, only one set of the generalized coordinates, which consists of either $q_{nuc}(t)$, $q_{nvs}(t)$, $q_{nwc}(t)$, or $q_{nus}(t)$, $q_{nvc}(t)$, $q_{nws}(t)$, is needed for the free vibration analysis. However, the full set of the generalized coordinates is necessary for control design because the actuator and sensor can be placed at any location along the circumference of the shell. This fact has not been fully explained in the previous studies.

Before inserting Eq. (6) into Eqs. (1) and (5), let us introduce non-dimensional variables for the ease of numerical analysis.

$$\xi = x/L, \quad \alpha = L/R, \quad \beta = h/R \tag{8a–c}$$

Considering that the displacements are expressed in terms of n functions corresponding to each circumferential mode, the kinetic and potential energies can be also expressed as

$$T = \sum_{n=0}^{\infty} T_n, \quad V = \sum_{n=0}^{\infty} V_n \tag{9a,b}$$

where T_n and V_n are the kinetic and potential energies corresponding to the nth circumferential mode, respectively. Considering Eq. (8) and inserting Eq. (6) into Eqs. (1) and (5), the kinetic and potential energies corresponding to the $n(\geqslant 1)$th circumferential mode can be derived as follows:

$$\begin{aligned} T_n = \frac{1}{2}\rho RhL\pi(&\dot{q}_{nuc}^T M_{uu}\dot{q}_{nuc} + \dot{q}_{nvs}^T M_{vv}\dot{q}_{nvs} + \dot{q}_{nwc}^T M_{ww}\dot{q}_{nwc} \\ &+ \dot{q}_{nus}^T M_{uu}\dot{q}_{nus} + \dot{q}_{nvc}^T M_{vv}\dot{q}_{nvc} + \dot{q}_{nws}^T M_{ww}\dot{q}_{nws}) \end{aligned} \tag{10}$$

$$\begin{aligned} V_n = \frac{\pi ERh}{(1-\nu^2)L}\Big(&\frac{1}{2}q_{nuc}^T K_{nuu}q_{nuc} + \frac{1}{2}q_{nvs}^T K_{nvv}q_{nvs} + \frac{1}{2}q_{nwc}^T K_{nww}q_{nwc} \\ &+ q_{nuc}^T K_{nuv}q_{nvs} + q_{nvs}^T K_{nvw}q_{nwc} + q_{nuc}^T K_{nuw}q_{nwc} \\ &+ \frac{1}{2}q_{nus}^T K_{nuu}q_{nus} + \frac{1}{2}q_{nvc}^T K_{nvv}q_{nvc} + \frac{1}{2}q_{nws}^T K_{nww}q_{nws} \\ &+ q_{nus}^T K_{nuv}q_{nvc} + q_{nvc}^T K_{nvw}q_{nws} + q_{nus}^T K_{nuw}q_{nws}\Big) \end{aligned} \tag{11}$$

where

$$M_{uu} = \Phi_{uu}, \quad M_{vv} = \Phi_{vv}, \quad M_{ww} = \Phi_{ww} \tag{12a–c}$$

$$K_{nuu} = \bar{\Phi}_{uu} + (1-\nu)\alpha^2 n^2 \Phi_{uu}/2, \quad K_{nvv} = \alpha^2 n^2 \Phi_{vv} + (1-\nu)\bar{\Phi}_{vv}/2 \tag{12d,e}$$

$$K_{nww} = \alpha^2 \Phi_{ww} + \frac{\beta^2}{12}\left(\frac{\hat{\Phi}_{ww}}{\alpha^2} + \alpha^2 n^4 \Phi_{ww} - 2\nu n^2 \tilde{\Phi}_{ww} + 2(1-\nu)n^2 \hat{\Phi}_{ww}\right) \tag{12f}$$

$$K_{nuv} = \nu n\alpha \tilde{\Phi}_{uv} - \frac{(1-\nu)\alpha n}{2}\hat{\Phi}_{uv}, \quad K_{nuw} = \nu\alpha \tilde{\Phi}_{uw}, \quad K_{nvw} = \alpha^2 n \Phi_{vw} \tag{12g–i}$$

in which

$$\Phi_{uu} = \int_0^1 \Phi_u^T \Phi_u \, \mathrm{d}\xi, \quad \Phi_{vv} = \int_0^1 \Phi_v^T \Phi_v \, \mathrm{d}\xi, \quad \Phi_{ww} = \int_0^1 \Phi_w^T \Phi_w \, \mathrm{d}\xi, \quad \Phi_{vw} = \int_0^1 \Phi_v^T \Phi_w \, \mathrm{d}\xi \tag{13a–d}$$

$$\bar{\Phi}_{uu} = \int_0^1 \Phi_u'^T \Phi_u' \, \mathrm{d}\xi, \quad \bar{\Phi}_{vv} = \int_0^1 \Phi_v'^T \Phi_v' \, \mathrm{d}\xi, \quad \bar{\Phi}_{ww} = \int_0^1 \Phi_w'^T \Phi_w' \, \mathrm{d}\xi, \quad \tilde{\Phi}_{uv} = \int_0^1 \Phi_u'^T \Phi_v \, \mathrm{d}\xi \tag{13e–h}$$

$$\tilde{\Phi}_{uw} = \int_0^1 \Phi_u'^T \Phi_w \, \mathrm{d}\xi, \quad \tilde{\Phi}_{ww} = \int_0^1 \Phi_w''^T \Phi_w \, \mathrm{d}\xi, \quad \hat{\Phi}_{uv} = \int_0^1 \Phi_u^T \Phi_v' \, \mathrm{d}\xi, \quad \hat{\Phi}_{ww} = \int_0^1 \Phi_w''^T \Phi_w'' \, \mathrm{d}\xi \tag{13i–l}$$

3. MFC actuator and sensor modelling

The MFC actuator considered in this study can be assumed as a unidirectional actuator since it consists of piezoceramic rods and therefore, it can be modelled as a pin-force model [11]. Due to the direction of the pin force, the actuating force generated by the MFC on the vibration mode of the shell varies with the orientation of the MFC actuator, as shown in Fig. 2. In this study, two cases in which the MFC actuator is glued to a cylindrical shell in either longitudinal or circumferential directions are considered, and the corresponding piezoelectric sensor and actuator equations are to be derived.

Based on the pin-force model [11], the actuating force produced by the MFC actuator can be expressed as:

$$f_{pa}^i = E_p d_{33} V_{pa}^i \tag{14}$$

where E_p is the Young's modulus of the piezoelectric material, d_{33} is the piezoelectric constant, and V_{pa}^i is the applied voltage to the MFC actuator, respectively.

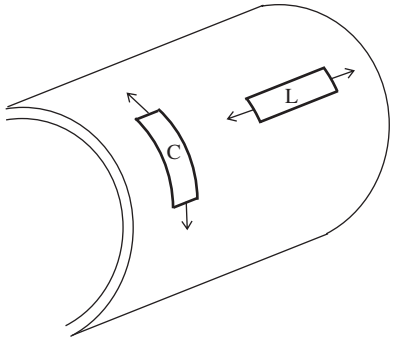

Fig. 2. Orientations of the MFC actuator.

3.1. MFC actuator aligned in the longitudinal direction

If the MFC actuator is glued to the cylindrical shell in the longitudinal direction, the surface displacement of the shell corresponding to the actuator can be expressed as

$$\bar{u} = u - \left(\frac{h}{2}\right)\frac{\partial w}{\partial x} \tag{15}$$

Using Eqs. (14) and (15), the virtual work for the circumferential mode ($n \geqslant 1$) can be expressed as

$$\delta W^i_{Ln} = \delta q^T_{nuc}(b^i_{Lanuc})^T V^i_{pa} + \delta q^T_{nwc}(b^i_{Lanwc})^T V^i_{pa} + \delta q^T_{nus}(b^i_{Lanus})^T V^i_{pa} + \delta q^T_{nws}(b^i_{Lanws})^T V^i_{pa} \tag{16}$$

where

$$b^i_{Lanuc} = \frac{E_p d_{33} R}{n}(\sin n\theta^i_{pae} - \sin n\theta^i_{pas})\,[\Phi_u(x^i_{pae}) - \Phi_u(x^i_{pas})] \tag{17a}$$

$$b^i_{Lanwc} = -\frac{E_p d_{33} Rh}{2n}(\sin n\theta^i_{pae} - \sin n\theta^i_{pas})\left[\frac{\mathrm{d}\Phi_w(x^i_{pae})}{\mathrm{d}x} - \frac{\mathrm{d}\Phi_w(x^i_{pas})}{\mathrm{d}x}\right] \tag{17b}$$

$$b^i_{Lanus} = -\frac{E_p d_{33} R}{n}(\cos n\theta^i_{pae} - \cos n\theta^i_{pas})\,[\Phi_u(x^i_{pae}) - \Phi_u(x^i_{pas})] \tag{17c}$$

$$b^i_{Lanws} = \frac{E_p d_{33} Rh}{2n}(\cos n\theta^i_{pae} - \cos n\theta^i_{pas})\left[\frac{\mathrm{d}\Phi_w(x^i_{pae})}{\mathrm{d}x} - \frac{\mathrm{d}\Phi_w(x^i_{pas})}{\mathrm{d}x}\right] \tag{17d}$$

where x^i_{pas} and x^i_{pae} are the starting and ending positions of the ith MFC actuator in the x direction and θ^i_{pas} and θ^i_{pae} are the angular positions of the ith MFC actuator. The piezoelectric sensor equation can be expressed as

$$V^i_L = -\frac{1}{C^i_c}\sum_{n=1}^{\infty}(b^i_{Lsnuc}q_{nuc} + b^i_{Lsnwc}q_{nwc} + b^i_{Lsnus}q_{nus} + b^i_{Lsnws}q_{nws}) \tag{18}$$

where $C_c{}^i$ represents the capacitance of the charge amplifier and

$$b^i_{Lsnuc} = \frac{E_p d_{33} R}{n}(\sin n\theta^i_{pse} - \sin n\theta^i_{pss})[\Phi_u(x^i_{pse}) - \Phi_u(x^i_{pss})] \tag{19a}$$

$$b^i_{Lsnwc} = -\frac{E_p d_{33} Rh}{2n}(\sin n\theta^i_{pse} - \sin n\theta^i_{pss})\left[\frac{\mathrm{d}\Phi_w(x^i_{pse})}{\mathrm{d}x} - \frac{\mathrm{d}\Phi_w(x^i_{pss})}{\mathrm{d}x}\right] \tag{19b}$$

$$b^i_{Lsnus} = -\frac{E_p d_{33} R}{n}(\cos n\theta^i_{pse} - \cos n\theta^i_{pss})\,[\Phi_u(x^i_{pse}) - \Phi_u(x^i_{pss})] \tag{19c}$$

$$b^i_{Lsnws} = \frac{E_p d_{33} Rh}{2n}(\cos n\theta^i_{pse} - \cos n\theta^i_{pss})\left[\frac{\mathrm{d}\Phi_w(x^i_{pse})}{\mathrm{d}x} - \frac{\mathrm{d}\Phi_w(x^i_{pss})}{\mathrm{d}x}\right] \tag{19d}$$

3.2. MFC actuator aligned in the circumferential direction

If the MFC actuator is glued to the cylindrical shell in the circumferential direction, the surface displacement of the shell corresponding to the actuator can be expressed as

$$\bar{v} = v + w\theta - \left(\frac{h}{2R}\right)\frac{\partial w}{\partial \theta} \tag{20}$$

Using Eqs. (14) and (20), the virtual work done by the actuator for the nth ($n \geqslant 1$) circumferential mode can be expressed as

$$\delta W^i_{Cn} = \delta q^T_{nvs}(b^i_{Canvs})^T V^i_{pa} + \delta q^T_{nwc}(b^i_{Canwc})^T V^i_{pa} + \delta q^T_{nvc}(b^i_{Canvc})^T V^i_{pa} + \delta q^T_{nws}(b^i_{Canws})^T V^i_{pa} \tag{21}$$

where

$$b^i_{Canvs} = E_p d_{33}(\sin n\theta^i_{pae} - \sin n\theta^i_{pas}) \int_{x^i_{pas}}^{x^i_{pae}} \Phi_v \, \mathrm{d}x \tag{22a}$$

$$b^i_{Canwc} = E_p d_{33}[(\theta^i_{pae} \cos n\theta^i_{pae} - \theta^i_{pas} \cos n\theta^i_{pas}) + \frac{nh}{2R}(\sin n\theta^i_{pae} - \sin n\theta^i_{pas})] \int_{x^i_{pas}}^{x^i_{pae}} \Phi_w \, \mathrm{d}x \tag{22b}$$

$$b^i_{Canvc} = E_p d_{33}(\cos n\theta^i_{pae} - \cos n\theta^i_{pas}) \int_{x^i_{pas}}^{x^i_{pae}} \Phi_v \, \mathrm{d}x \tag{22c}$$

$$b^i_{Canws} = E_p d_{33}[(\theta^i_{pae} \sin n\theta^i_{pae} - \theta^i_{pas} \sin n\theta^i_{pas}) - \frac{nh}{2R}(\cos n\theta^i_{pae} - \cos n\theta^i_{pas})] \int_{x^i_{pas}}^{x^i_{pae}} \Phi_w \, \mathrm{d}x \tag{22d}$$

And the piezoelectric sensor equation for this case can be expressed as

$$V^i_C = -\frac{1}{C^i_c} \sum_{n=1}^{\infty} (b^i_{Csnvs} q_{nvs} + b^i_{Csnwc} q_{nwc} + b^i_{Csnvc} q_{nvc} + b^i_{Csnws} q_{nws}) \tag{23}$$

where

$$b^i_{Csnvs} = E_p d_{33}(\sin n\theta^i_{pse} - \sin n\theta^i_{pss}) \int_{x^i_{pss}}^{x^i_{pse}} \Phi_v \, \mathrm{d}x \tag{24a}$$

$$b^i_{Csnwc} = E_p d_{33}[(\theta^i_{pse} \cos n\theta^i_{pse} - \theta^i_{pss} \cos n\theta^i_{pss}) + \frac{nh}{2R}(\sin n\theta^i_{pse} - \sin n\theta^i_{pss})] \int_{x^i_{pss}}^{x^i_{pse}} \Phi_w \, \mathrm{d}x \tag{24b}$$

$$b^i_{Csnvc} = E_p d_{33}(\cos n\theta^i_{pse} - \cos n\theta^i_{pss}) \int_{x^i_{pss}}^{x^i_{pse}} \Phi_v \, \mathrm{d}x \tag{24c}$$

$$b^i_{Csnws} = E_p d_{33}[(\theta^i_{pse} \sin n\theta^i_{pse} - \theta^i_{pss} \sin n\theta^i_{pss}) - \frac{nh}{2R}(\cos n\theta^i_{pse} - \cos n\theta^i_{pss})] \int_{x^i_{pss}}^{x^i_{pse}} \Phi_w \, \mathrm{d}x \tag{24d}$$

4. Equations for motion and sensing

Inserting Eqs. (9), (10) and (11) and either (16) or (21) into Lagrange's equation, the equations of motion of the cylindrical shell for the nth circumferential mode can be derived.

$$M^* \ddot{q}_n + K^*_n q_n = B^*_n V_{pa}, \quad n = 1, 2, \ldots \tag{25}$$

where $q_n(t) = [q^T_{n1} \; q^T_{n2}]^T$ is the generalized coordinate vector consisting of $q_{n1}(t) = [q^T_{nuc} \; q^T_{nvs} \; q^T_{nwc}]^T$ and $q_{n2}(t) = [q^T_{nus} \; q^T_{nvc} \; q^T_{nws}]^T$ and

$$M^* = \rho R h L \pi \begin{bmatrix} M & 0 \\ 0 & M \end{bmatrix}, \quad K^*_n = \frac{ERh\pi}{(1-\nu^2)L} \begin{bmatrix} K_n & 0 \\ 0 & K_n \end{bmatrix} \tag{26}$$

are mass and stiffness matrices. Identical matrices appear in the mass and stiffness matrices of Eq. (26) because they belong to the sine and cosine modes, respectively. Furthermore,

$$M = \begin{bmatrix} M_{uu} & 0 & 0 \\ 0 & M_{vv} & 0 \\ 0 & 0 & M_{ww} \end{bmatrix}, \quad K_n = \begin{bmatrix} K_{nuu} & K_{nuv} & K_{nuw} \\ K_{nuv}^{\mathrm{T}} & K_{nvv} & K_{nvw} \\ K_{nuw}^{\mathrm{T}} & K_{nvw}^{\mathrm{T}} & K_{nww} \end{bmatrix} \tag{27a,b}$$

and B_n^* is the force participation matrix, which reflects the effect of the applied voltage on each mode. For example, if the first actuator is attached to the cylindrical shell in the longitudinal direction and the second actuator is attached to the cylindrical shell in the circumferential direction, then the force participation matrix can be expressed as

$$B_n^* = \begin{bmatrix} (b_{Lanuc}^1)^T & 0 & \cdots \\ 0 & (b_{Canvs}^2)^T & \cdots \\ (b_{Lanwc}^1)^T & (b_{Canwc}^2)^T & \cdots \\ (b_{Lanus}^1)^T & 0 & \cdots \\ 0 & (b_{Canvc}^2)^T & \cdots \\ (b_{Lanws}^1)^T & (b_{Canws}^2)^T & \cdots \end{bmatrix} \tag{28}$$

It becomes evident from Eqs. (25) and (26) that all cosine and sine modes are necessary for control design because the resulting displacements, u,v,w, are the combination of sine and cosine circumferential modes. Using the piezoelectric sensor equations for the longitudinal and circumferential alignments, Eqs. (18) and (23), the resulting piezoelectric sensor equation can be expressed as

$$V_{ps} = \sum_{n=1}^{\infty} C_n^* q_n \tag{29}$$

where C_n^* is the mode influence matrix, which reflects the effect of each mode on the sensor voltage. For example, if the first sensor is attached to the cylindrical shell in the longitudinal direction and the second sensor is attached to the cylindrical shell in the circumferential direction, the mode influence matrix can be expressed as

$$C_n^* = -\begin{bmatrix} b_{Lsnuc}^1/C_{c1} & 0 & b_{Lsnwc}^1/C_{c1} & b_{Lsnus}^1/C_{c1} & 0 & b_{Lsnws}^1/C_{c1} \\ 0 & b_{Csnvs}^2/C_{c2} & b_{Csnwc}^2/C_{c2} & 0 & b_{Csnvc}^2/C_{c2} & b_{Csnws}^2/C_{c2} \\ \vdots & \vdots & \vdots & \vdots & \vdots & \vdots \end{bmatrix} \tag{30}$$

5. Eigenvalue analysis and experiment

Eq. (25) results in an eigenvalue problem for the nth circumferential mode.

$$|K_n^* - \omega^2 M^*| = 0 \tag{31}$$

Eq. (31) reduces to the following equation because of the duplicates in the mass and stiffness matrices.

$$|K_n - \bar{\omega}^2 M| = 0 \tag{32}$$

where $\bar{\omega} = \omega\sqrt{\rho(1-\nu^2)L^2/E}$ represents the non-dimensionalized natural frequency. The dimension of the matrices in Eq. (32) is half of the dimension of the matrices in Eq. (31). Hence, the free vibration analysis based on Eq. (32) is preferred.

An aluminium cylindrical shell shown in Fig. 3 was manufactured for this study. Its thickness, inner diameter, and length are 2, 250, and 500 mm, respectively. The material properties of the aluminium used in this study are $\rho = 2770\,\mathrm{kg/m^3}$, $\nu = 0.3$, $E = 70\,\mathrm{GPa}$. As shown in Fig. 3, the supporting thick circular plates

Fig. 3. Aluminium cylindrical shell.

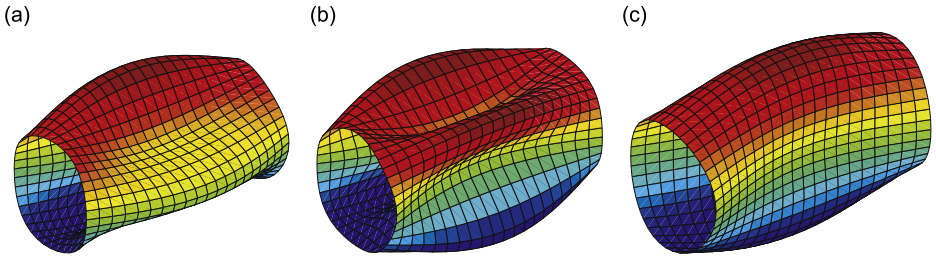

Fig. 4. Natural mode shapes.

are mounted on the flanges of the cylindrical shell so that the shear diaphragm boundary condition at both ends is assumed for the theoretical analysis, i.e.,

$$v = w = M_x = N_x = 0 \tag{33}$$

The admissible functions which satisfy the above boundary conditions can be expressed as [2]

$$\Phi_{ui}(x) = \sqrt{2}\cos\frac{i\pi x}{L}, \quad \Phi_{vi}(x) = \Phi_{wi}(x) = \sqrt{2}\sin\frac{i\pi x}{L}, \quad i = 1, 2, \ldots, m \tag{34}$$

Inserting Eq. (34) into Eq. (13) and inserting the results into Eq. (12) ,we can obtain the mass and stiffness matrices of Eq. (27) for each nth circumferential mode. Numerical results showed that the natural frequencies of the cylindrical shell were 479 Hz (3,1), 549 Hz (4,1), 767 Hz (2,1), 792 Hz (5,1), 1005 Hz (5,2), 1342 Hz (3,2), 1124 Hz (6,1), where the numbers in the parenthesis represent the nth circumferential mode and the order in that mode. Fig. 4 shows the first three natural modes. Modal testing was carried out using an accelerometer and impact hammer. Fig. 5 shows the frequency response curve obtained by experiments. The natural frequencies obtained by experiment were 486, 616, 690, 912, 1028, and 1128 Hz. The first and second theoretical natural frequencies are close to the experimental ones but the higher theoretical natural frequencies are not in good agreement with experimental ones, which seems due to the incompleteness of the shear diaphragm boundary condition. The same observation was made by the finite element analysis [10] for the end-capped shell.

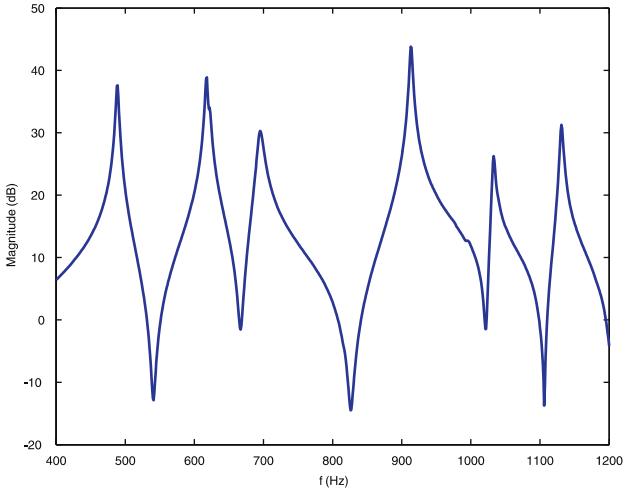

Fig. 5. Experimental frequency response curve.

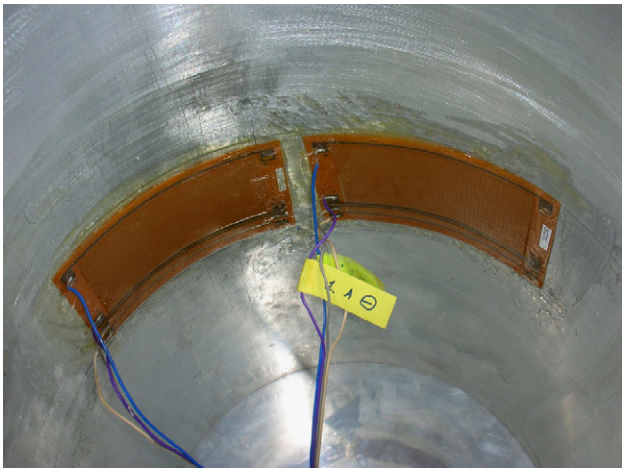

Fig. 6. MFC actuators mounted on the aluminium shell.

6. Controller design and experiment

In this study, the first two natural modes of vibration are to be controlled. To this end, two MFC actuators were glued to the cylindrical shell, as shown in Fig. 6, in circumferential direction because the circumferential modes are dominant due to the high radius-to-length ratio so that the piezoelectric actuator attached in the circumferential direction is more effective than the one attached in the longitudinal direction. The MFC actuator used in this study is the M8557S1 actuator of Smart Materials Inc. [9] and its piezoelectric type is Navy Type II. The dimension of the MFC actuator is $110\,\text{mm} \times 75\,\text{mm}$ and consists of an actuator ($110\,\text{mm} \times 75\,\text{mm}$) and sensor ($85\,\text{mm} \times 50\,\text{mm}$). The material properties of the MFC actuator are $E_1 = 30.34\,\text{GPa}$, $E_2 = 15.86\,\text{GPa}$ (electrode direction), $\nu_{12} = 0.31$, $\nu_{21} = 0.16$, $G_{12} = 5.52\,\text{GPa}$. The most important parameter is the piezoelectric constant. The MFC actuator uses d_{33} to produce more actuating force than the one using d_{31}. The piezoelectric constant found in the specification is $d_{33} = 4.6 \times 10^2\,\text{pm/V}$.

The equations of motion of the cylindrical shell given by Eq. (25) and the piezoelectric sensor equations given by Eq. (29) include infinite number of modes and thus are not suitable for control design. In addition, natural frequencies found both theoretically and experimentally are very high for digital control implementation; therefore, many natural modes of the cylindrical shell structure are uncontrollable

practically. Therefore, the reduced-order dynamic model is preferred for efficient control design. After solving the eigenvalue problem corresponding to the nth circumferential mode independently, the eigenvalue and eigenvector are obtained. They satisfy the orthonormality condition.

$$U_n^T M^* U_n = I, \quad U_n^T K_n^* U_n = \Lambda_n \tag{35}$$

where $\Lambda_n = diag([\omega_{n1}^2\ \omega_{n1}^2\ \omega_{n2}^2\ \omega_{n2}^2 \ldots])$ is the eigenvalue matrix and U_n is the eigenvector matrix. Using Eq. (35) and the modal transformation, $q_n = U_n\ p_n$, Eqs. (25) and (29) can be converted to the modal equations of motion and modal sensor equation

$$\ddot{p}_n + \Lambda_n p_n = \overline{B}_n^* V_{pa}, \quad n = 1, 2, \ldots, \quad V_{ps} = \sum_{n=1}^{\infty} \overline{C}_n^* p_n \tag{36a,b}$$

where $\overline{B}_n^* = U_n^T B_n^*$ and $\overline{C}_n^* = C_n^* U_n$. After rearranging Eq. (36) in the ascending order of natural frequency, let us consider m vibration modes to be controlled and add damping terms to the equations of motion. Then, we can obtain the following reduced-order modal equations of motion and the modal sensor equation.

$$\ddot{\xi} + 2Z\Omega\dot{\xi} + \Lambda\xi = B_a v_a, \quad v_s = C_s\xi \tag{37}$$

where $\xi = [\xi_{11}\ \xi_{12}\ \xi_{21}\ \xi_{22} \cdots \xi_{m1}\ \xi_{m2}]^{\mathrm{T}}$ represents the generalized coordinate for the vibration mode, Z is the matrix consisting of damping factors, Ω is the diagonal matrix consisting of natural frequencies, Λ is the diagonal matrix consisting of the square of the natural frequency, B_a and C_s are the matrices of force participation and mode influence, respectively. Since the same natural frequency and mode belong to the sine and cosine circumferential modes, a pair of generalized coordinates belongs to the same natural frequency. Therefore, Z, Ω, Λ in Eq. (37) are expressed as follows:

$$Z = \begin{bmatrix} \zeta_1 & 0 & 0 & 0 & \cdots & 0 \\ 0 & \zeta_1 & 0 & 0 & \cdots & 0 \\ 0 & 0 & \zeta_2 & 0 & \cdots & 0 \\ 0 & 0 & 0 & \zeta_2 & \cdots & 0 \\ \vdots & \vdots & \vdots & \vdots & \ddots & \vdots \\ 0 & 0 & 0 & 0 & 0 & \zeta_m \end{bmatrix}, \quad \Omega = \begin{bmatrix} \omega_1 & 0 & 0 & 0 & \cdots & 0 \\ 0 & \omega_1 & 0 & 0 & \cdots & 0 \\ 0 & 0 & \omega_2 & 0 & \cdots & 0 \\ 0 & 0 & 0 & \omega_2 & \cdots & 0 \\ \vdots & \vdots & \vdots & \vdots & \ddots & \vdots \\ 0 & 0 & 0 & 0 & 0 & \omega_m \end{bmatrix}, \quad \Lambda = \Omega^2 \tag{38a–c}$$

If a small number of natural modes is to be controlled, Eq. (37) represents the reduced-order equations of motion for the shell structure. Eq. (37) is a new kind of structural vibration control problem because of duplicate natural modes. For instance, the resulting equations of motion turn out to be a four degrees-of-freedom model for the control of two natural modes with two sensors and two actuators.

Let us design the active vibration controller based on Eq. (37) which can suppress the first two natural modes with two sensors and two actuators. The control algorithm adopted in this study is the MIMO PPF control based on the block-inverse technique [12], which proved to be useful in controlling more modes with a limited number of sensors and actuators. In this case, we can rewrite Eq. (37) as

$$\begin{Bmatrix} \ddot{\xi}_1 \\ \ddot{\xi}_2 \end{Bmatrix} + \begin{bmatrix} 2Z_1\Omega_1 & 0 \\ 0 & 2Z_2\Omega_2 \end{bmatrix} \begin{Bmatrix} \dot{\xi}_1 \\ \dot{\xi}_2 \end{Bmatrix} + \begin{bmatrix} \Lambda_1 & 0 \\ 0 & \Lambda_2 \end{bmatrix} \begin{Bmatrix} \xi_1 \\ \xi_2 \end{Bmatrix} = \begin{bmatrix} B_{a1} \\ B_{a2} \end{bmatrix} \begin{Bmatrix} v_{a1} \\ v_{a2} \end{Bmatrix},$$
$$\begin{Bmatrix} v_{s1} \\ v_{s2} \end{Bmatrix} = [C_{s1}\ \ C_{s2}] \begin{Bmatrix} \xi_1 \\ \xi_2 \end{Bmatrix} \tag{39}$$

where $\xi_i = [\xi_{i1}\ \xi_{i2}]$, $i = 1,2$ and

$$Z_i = \begin{bmatrix} \zeta_i & 0 \\ 0 & \zeta_i \end{bmatrix}, \quad \Omega_i = \begin{bmatrix} \omega_i & 0 \\ 0 & \omega_i \end{bmatrix}, \quad \Lambda_i = \begin{bmatrix} \omega_i^2 & 0 \\ 0 & \omega_i^2 \end{bmatrix}, \quad i = 1, 2 \tag{40a–c}$$

Based on the result of Kwak and Heo [12], the MIMO PPF controller for Eq. (39) in the s domain can be expressed as

$$V_a(s) = B_a^* G^{1/2} \Lambda^* H_{ppf}(s) G^{1/2} C_s^* V_s(s) \tag{41}$$

where G is the 4×4 gain matrix and

$$B_a^* = [B_{a1}^{-1} \;\; B_{a2}^{-1}], \quad C_s^* = \begin{bmatrix} C_{s1}^{-1} \\ C_{s2}^{-1} \end{bmatrix} \tag{42a,b}$$

$$\Lambda^* = \begin{bmatrix} \Lambda_1 & 0 \\ 0 & \Lambda_2 \end{bmatrix}, \quad H_{ppf}(s) = \begin{bmatrix} H_1(s) & 0 & 0 & 0 \\ 0 & H_1(s) & 0 & 0 \\ 0 & 0 & H_2(s) & 0 \\ 0 & 0 & 0 & H_2(s) \end{bmatrix} \tag{42c,d}$$

in which

$$H_i(s) = \frac{\omega_{fi}^2}{s^2 + 2\zeta_f \omega_{fi} s + \omega_{fi}^2}, \quad i = 1, 2 \tag{43}$$

is the single-input and single-output PPF controller for each mode. ζ_f, ω_{fi} are the filter damping factor and frequency of the single-input and single-output PPF controller. In the experiment, the filter frequencies of the PPF controllers were tuned to the natural frequencies of the cylindrical shell, which were found experimentally. In general, the filter damping factor, ζ_f, is set to 0.3, which was also used in this study.

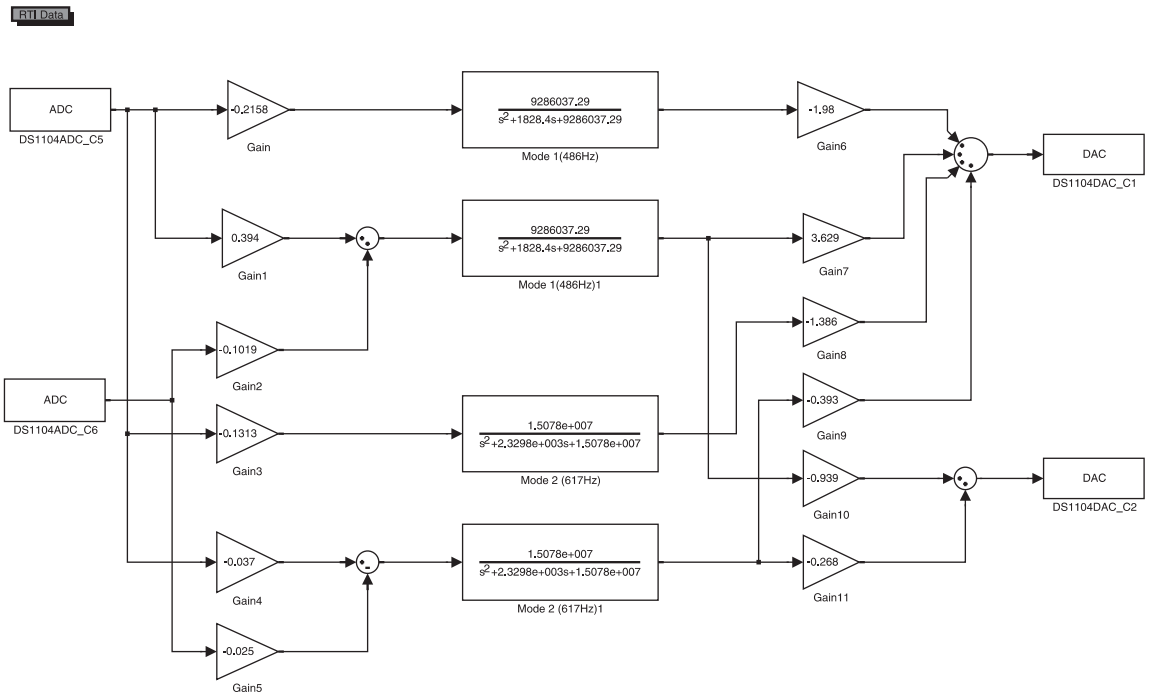

Fig. 7. Simulink block diagrams for MIMO PPF control.

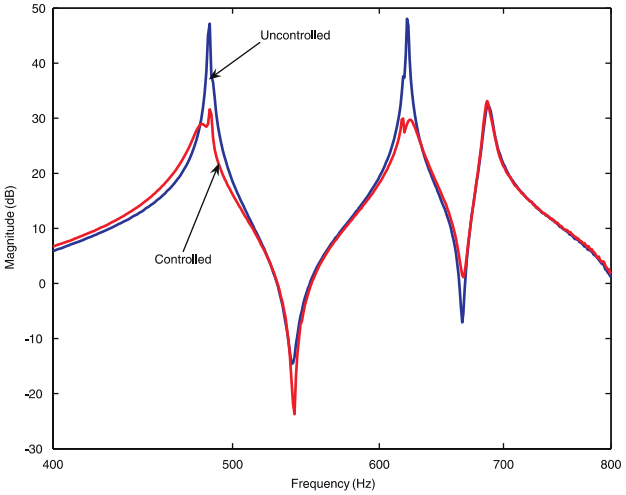

Fig. 8. Uncontrolled and controlled frequency response plots from experiments.

The matrices of force participation and mode influence are computed theoretically as follows based on the dimensions and material properties of the cylindrical shell and the MFC actuator.

$$B_a^* G \Lambda^* = 10^5 \begin{bmatrix} -1.9873 & 3.6295 & -1.3862 & -0.3931 \\ 0 & -0.9391 & 0 & -0.2684 \end{bmatrix},$$

$$C_s^* = 10^{-5} \begin{bmatrix} -0.2158 & 0 \\ 0.3942 & -0.1020 \\ -0.1314 & 0 \\ -0.0372 & -0.0254 \end{bmatrix} \tag{44a,b}$$

The active vibration controller, Eq. (41), along with Eq. (44) was implemented digitally by using the DS1103 of dSpace Inc [13] with 5 kHz sampling rate. Fig. 7 shows the Simulink [14] block diagram for the active vibration controller given by Eqs. (41) and (44). Fig. 8 shows the uncontrolled and controlled frequency response curves obtained by experiments. Fig. 8 shows that about 20 dB reductions are obtained for the natural frequencies at 479 and 549 Hz. Hence, it can be concluded that the active vibration controller developed in this study was successful in suppressing the vibrations of the cylindrical shell. Fig. 9 shows the time response of the sensor output, when the actuator was powered approximately 0.2 s after impact. The response was suppressed rapidly after the control was applied, as shown in Fig. 9.

7. Summary and conclusions

In this study, dynamic modelling and active vibration control design for the cylindrical shell structure equipped with piezoelectric sensors and actuators were discussed. The equations of motion for the cylindrical shell and the piezoelectric sensor equations in matrix forms, which are suitable for control design, were derived using the Rayleigh–Ritz method by assuming the piezoelectric actuator as a pin-force model. Free vibration analysis on the cylindrical shell was carried out, and its results were compared to experimental results, which showed that the first two natural frequencies of the theoretical model are in good agreement with the measured natural frequencies but the higher natural frequencies of the theoretical model differ from the measured natural frequencies. The discrepancy between the theoretical and experimental results seems to be due to incompleteness of the shear diaphragm boundary condition considered in the theoretical model. In fact, the flanges and cover plates give more constraint on the boundary of the cylindrical shell than the shear diaphragm does.

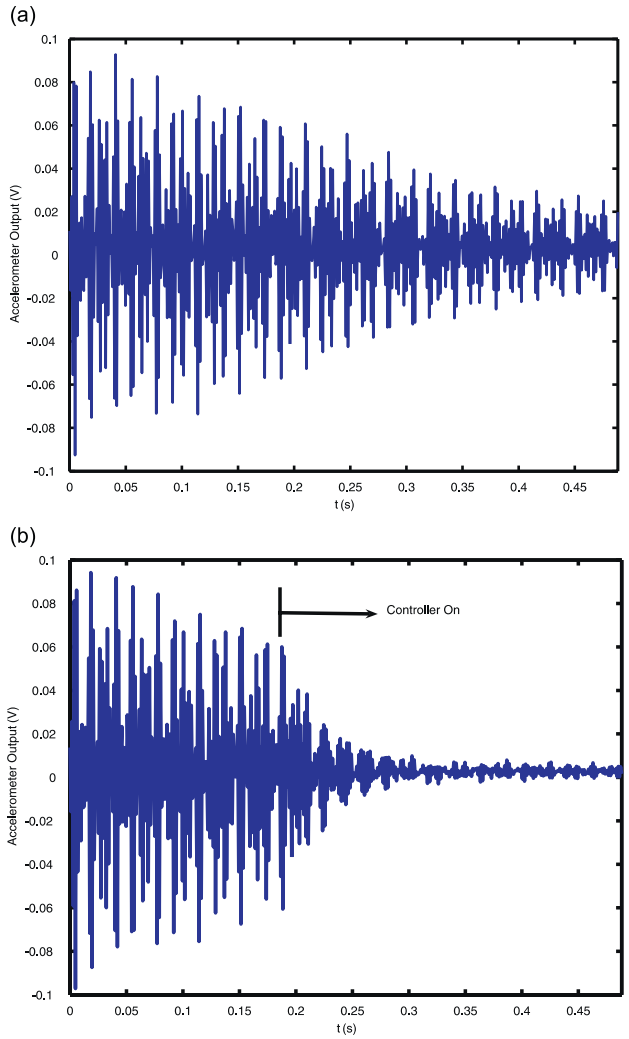

Fig. 9. (a) Uncontrolled and (b)controlled time responses of accelerometer output.

A reduced-order model was derived considering the lowest natural modes from the equations of motion for each circumferential mode because the infinite number of equations of motion is not suitable for control design. The procedure for reducing the equations of motion for the cylindrical shell structure is explained in detail. Also, a new MIMO PPF control scheme was proposed to suppress modes belonging to the same natural frequency.

The MFC actuator which consists of piezoelectric sensor and actuator in one wafer was considered in experiment. Two MFC actuators were glued to the aluminium shell for active vibration control and the MIMO PPF controller was designed and implemented digitally using the DSP board. The experimental results showed that vibrations of the cylindrical shell were suppressed successfully by the piezoelectric sensors and actuators.

Acknowledgements

This study was supported by research grant from the Underwater Vehicle Research Center of Defense Acquisition Program Administration and Agency for Defense Development, Korea. This financial support is gratefully acknowledged.

References

[1] R.N. Arnold, G.B. Waburton, Flexural vibrations of the walls of thin cylindrical shells having freely supported ends, *Proceedings of the Royal Society of London, Series A* 197 (1949) 238–256.
[2] A. Leissa, *Vibration of Shells*, Acoustical Society of America, Originally issued by NASA 1973, (1993).
[3] J. Yuan, S.M. Dickinson, The free vibration of circularly cylindrical shell and plate systems, *Journal of Sound and Vibration* 175 (2) (1994) 241–263.
[4] S. Markus, *The Mechanics of Vibrations of Cylindrical Shells, Studies in Applied Mechanics*, Vol. 17, Elsevier, 1988.
[5] H.S. Tzou, J.P. Zhong, J.J. Hollkamp, Spatially distributed orthogonal piezoelectric shell actuator: theory and applications, *Journal of Sound and Vibration* 188 (1994) 363–378.
[6] H.C. Lester, S. Lefebvre, Piezoelectric actuator models for active sound and vibration control of cylinders, *Proceedings of the Conference on Recent Advances in Active Control of Sound and Vibration*, Virginia Polytechnic Institute and State University, Blacksburg, VA, 1991, pp. 3–26.
[7] V.R. Sonti, J.D. Jones, Active vibration control of thin cylindrical shells using piezo-electric actuators, *Proceedings of the Conference on Recent Advances in Active Control of Sound and Vibration*, Virginia Polytechnic Institute and State University, Blacksburg, VA, 1991, pp. 27–38.
[8] R.L. Clark, C.R. Fuller, Active control of structurally radiated sound from an enclosed finite cylinder, *Proceedings of the Conference on Recent Advances in Active Control of Sound and Vibration*, Virginia Polytechnic Institute and State University, Blacksburg, VA, 1991, pp. 380–402.
[9] 〈http://www.smart-material.com〉.
[10] J.W. Sohn, H.S. Kim, S.B. Choi, Dynamic modeling and vibration control of smart hull structure, *Transactions of the Korean Society for Noise and Vibration Engineering* 16 (8) (2006) 840–847.
[11] Z. Chaudhry, F. Lalande, C.A. Rogers, Modeling of induced strain actuation of shell structure, *Journal of the Acoustical Society of America* 97 (1995) 2872–2877.
[12] M.K. Kwak, S. Heo, Active vibration control of smart grid structure by multiinput and multioutput positive position feedback controller, *Journal of Sound and Vibration* 304 (2007) 230–245.
[13] 〈http://www.dspaceinc.com〉.
[14] 〈http://www.mathworks.com〉.